Engineering Transactions, **69**(3): 293–313, 2021, doi: 10.24423/EngTrans.1329.20210826
Polish Academy of Sciences • Institute of Fundamental Technological Research (IPPT PAN)
Université de Lorraine • Poznan University of Technology

Research Paper

An Investigation on the Effective Mass of the Robot: Dependence on the End-Effector Position

Abdel-Nasser SHARKAWY

Mechatronics Engineering, Mechanical Engineering Department
Faculty of Engineering, South Valley University
Qena, 83523, Egypt
e-mail: eng.abdelnassersharkawy@gmail.com

In this paper, the mathematical analysis of the robot effective mass is presented. The calculation of this effective mass and its ellipsoid are included. The relationship between the robot effective mass and the external force (collision) affecting the robot end-effector is investigated. The effective mass is analyzed using different robot configurations and different end-effector positions. This analysis is conducted using 2-DOF and 3-DOF planar robots and executed using MATLAB. The results from this analysis prove that the robot effective mass depends on the its configurations and end-effector position. Effective mass can thus be considered as one of the criteria in optimizing robot kinematics and configuration.

Key words: mathematical analysis; robot effective mass; ellipsoid; 2-DOF and 3-DOF robots.

1. Introduction

Starting from a rest position, the effective mass of robot [1] is equal to the inverse of the magnitude of the component of the linear acceleration along the direction u that results in response to a unit force applied along this direction. In this paper, the robot effective mass is investigated and presented using different positions of the robot end-effector.

Effective mass was used by many researchers in the area of safety of human-robot interaction. In [2], a collision model was implemented to evaluate any spatial manipulator's collision safety. This collision model relates the design parameters to collision safety by adopting the robot effective mass and manipulability. Chen *et al.* [3] designed a contact force minimization strategy using the effective mass for the space flexible manipulator. This strategy decreases the contact force by deriving the pre-configuration and collision direction. In [4], Mavrakis *et al.* investigated how the safety of the post-grasp motion could be considered in the phase of the pre-grasp approach so that the selected grasp is optimal in terms of applying the minimum impact forces for the collision occurring during

a desired post-grasp manipulation. Their research are based on the methods of the augmented robot-object dynamics models and the effective mass. A new mechanical safety coupling for human-robot cooperation using magnetorheological fluids was developed by Lämmle [5]. In this approach, decoupling the robot effective mass from the tool effective mass and potentially handled parts during the collision significantly reduced the transmitted energy upon the affected parts of the human body. Therefore, the injuries' risk was limited. In [6], a virtual sensor approach was presented, which computes the expected collision peak force and pressure that result from the collisions between the robot and the human. The collision safety was evaluated using the finite element simulation for the particular collision conditions with the given parameters such as the effective mass, the collision velocity, the impactor shape, and the collision direction. It was found that controlling the robot speed and/or altering its posture was necessary for reducing the effective mass to keep the collision force lower than the limit.

From these studies, we can conclude that the effective mass analysis of robots is of great significance in improving the safety of human-robot interaction and collaboration. However, investigation of the effective mass of the robot by using different positions of the robot end-effector is missing. Therefore, the robot effective mass deserves to be studied and investigated.

In this paper, the mathematical analysis of the robot effective mass is presented in detail. In this analysis, the relationship between the effective mass and the contact force is presented. The main contribution of this study is to investigate and identify the relationship between the robot effective mass and its end-effector position. For this purpose, the robot effective mass is calculated using different positions of the robot end-effector in x- and y-coordinates, assuming the z-coordinate is fixed. The 2-DOF and the 3-DOF planar robots are selected to be the case study for investigating the effective mass.

The rest of this paper is divided as follows: Sec. 2 presents the robot effective mass analysis and its ellipsoid. In Sec. 3, the relationship between the robot effective mass and the contact force is presented. Section 4 presents the analysis of the robot effective mass using different positions of the robot end-effector. This analysis is applied using MATLAB and 2-DOF and 3-DOF planar robots. Section 5 summarizes the main points of this work and outlines the directions for the future work.

2. Effective mass analysis and its ellipsoid

In this section, the robot effective mass and its ellipsoid are defined. The effective mass of the robot along the direction vector $\mathbf{u}$ is calculated from the following equation [1]:

$$m^{-1} = \mathbf{u}^{\mathrm{T}} \left(\mathbf{J}(q)\, \mathbf{M}(q)^{-1} \mathbf{J}^{\mathrm{T}}(q) \right) \mathbf{u} = \mathbf{u}^{T}\, \mathbf{H}^{-1}\, \mathbf{u}. \tag{2.1}$$

Therefore,

$$m = \frac{1}{\mathbf{u}^{\mathrm{T}}\, \mathbf{H}^{-1}\, \mathbf{u}}, \tag{2.2}$$

where $\mathbf{J}(q)$ is the Jacobian matrix of the manipulator, $\mathbf{M}(q)$ is the inertia matrix of the manipulator, and $\mathbf{u}$ is the direction vector, which describes the direction of the force applied to the robot end-effector.

Equation (2.2) shows that the robot effective mass is affected by its configuration and the direction of the collision.

The distribution law of the effective mass can be presented from Eq. (2.2) as follows [3]:

$$\widetilde{\mathbf{u}}^{\mathrm{T}}\, \mathbf{H}^{-1}\, \widetilde{\mathbf{u}} = 1, \tag{2.3}$$

where $\widetilde{\mathbf{u}} = \sqrt{m}\mathbf{u}$.

Equation (2.3) represents the ellipsoid of the robot effective mass. The principal axes of this ellipsoid are reciprocal to the square root of the corresponding eigenvalues of $\mathbf{H}^{-1}$, and the direction of each axis is consistent with the corresponding eigenvector.

The length of the longest and the shortest axis of the ellipsoid is given by [3]:

$$\|r\|_{\max} = \frac{1}{\sqrt{\lambda}_{\min}}, \qquad \|r\|_{\min} = \frac{1}{\sqrt{\lambda}_{\max}}, \tag{2.4}$$

where $\lambda_{\min}$ is the minimum eigenvalue of $\mathbf{H}^{-1}$, and $\lambda_{\max}$ is the maximum eigenvalue of $\mathbf{H}^{-1}$.

Because the robot configuration and its other structural parameters will determine the eigenvalues of $\mathbf{H}^{-1}$, these different configurations will produce ellipsoids of different sizes, and the lengths and directions of the principal axes of these ellipsoids will be different.

Furthermore, if $\mathbf{p}$ is a vector from the center of the ellipsoid to its surface in any direction and $\mathbf{p}_v$ is the unit vector coincident with $\mathbf{p}$, then the norm of $\mathbf{p}$ can be presented as follows [3]:

$$\|r\|_p = \frac{1}{\mathbf{p}_v^{\mathrm{T}}\, \mathbf{H}^{-1}\, \mathbf{p}_v}. \tag{2.5}$$

Since $\mathbf{p} = \sqrt{m}\, \mathbf{p}_v$, then the norm of $\mathbf{p}$ can be rewritten in the following form:

$$\|r\|_p = \sqrt{\mathbf{p}^{\mathrm{T}}\mathbf{p}} = \sqrt{m\, \mathbf{p}_v^{\mathrm{T}}\mathbf{p}_v} = \sqrt{m}\,. \tag{2.6}$$

Equations (2.5) and (2.6) are expressions of the distance from the ellipsoid center to its surface in a certain direction $\mathbf{p}_v$. Furthermore, the effective mass of the robot along this direction is the square of the distance, for example, $m = \|r\|_p^2$. Therefore, the smaller the distance from the center of the ellipsoid to its surface, the smaller the effective mass. Therefore, if the direction of collision coincides with the ellipsoid shortest axis, the effective mass of the manipulator will be the minimum, for example, $m = 1/\sqrt{\lambda}_{\max}$. If the collision direction coincides with the longest axis, the effective mass will reach the maximum, for example, $m = 1/\sqrt{\lambda}_{\min}$.

Hence, the configuration of the manipulator and the collision direction will both decide the effective mass. Figure 1 presents the ellipsoid of the effective mass when the robot collides with a target in the collision direction.

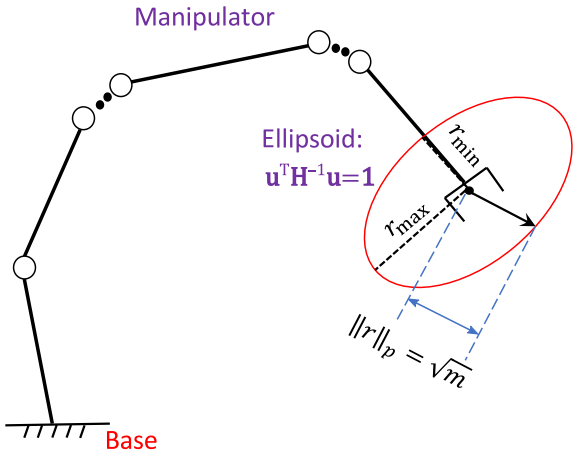

Fig. 1. The ellipsoid representation of the effective mass of the robot.

3. Effective mass vs. collision force

This section illustrates the relationship between the robot effective mass and the contact force.

The transferred energy to the human body during the physical collision with the robot systems is defined by [7]:

$$\Delta E = \frac{1}{2} M_t \, (V_i^2 - V_f^2), \tag{3.1}$$

where V_i is the relative impact velocity between the two colliding bodies just before the impact takes place. V_f represents the relative impact velocity between the two colliding bodies just before separating from each other. M_t is the total mass calculated from the effective mass of the robot and the human body.

Equation (3.1) can be rewritten according to [8] in the following form:

$$\Delta E = \frac{1}{2} M_t V_i^2 (1 - C_R^2), \tag{3.2}$$

where C_R is the restitution coefficient. M_t can be calculated from the following equation:

$$M_t = \left(\frac{1}{m} + \frac{1}{m_h} \right)^{-1} = \frac{m\, m_h}{m + m_h}, \tag{3.3}$$

where m_h is the effective mass of the human body, m is the effective mass of the robot and it is calculated from Eq. (2.2).

Assuming m_h is very large and, for example, is equal to infinity, therefore $M_t = \frac{m\, m_h}{m + m_h} \approx m$, so Eq. (3.2) can be rewritten in the following form:

$$\Delta E = \frac{1}{2}\, m\, V_i^2 \left(1 - C_R^2\right). \tag{3.4}$$

Using the principle of the work energy, the transferred energy can be presented in terms of work done as follows [9]:

$$\Delta E = F_c \delta_{\max}, \tag{3.5}$$

where F_c is the contact force due to the impact between the robot and the human body, and δ is the deformation during the contact process.

Therefore, Eq. (3.4) can be rewritten in the following form:

$$F_c \delta_{\max} = \frac{1}{2} m\, V_i^2 \left(1 - C_R^2\right). \tag{3.6}$$

Equation (3.6) links the contact force with the effective mass of the robot. From this equation, we conclude that the collision force depends on the robot effective mass. Reference [10] supports this conclusion.

During the impact between the robot and the human deformation can occur. Practically, the physical impact between the robot and the human is assumed to be completely inelastic for the worst-case scenario, where the kinetic energy is directly used to calculate the energy density [7]. The influence of the elastic properties of the human body regions will not be considered for the energy calculation. However, these properties need to be considered for calculating the contact area and the rate of contact deformation of the human soft tissues for power flux density estimation.

4. The effective mass analysis with different end-effector positions

In this section, an investigation of the robot effective mass by using different positions of the robot end-effector is presented. This analysis is performed using 2-DOF and 3-DOF planar robots. The analysis is carried out using MATLAB.

4.1. The effective mass analysis using 2-DOF robot

In this subsection, the effective mass of the 2-DOF manipulator (shown in Fig. 2) is presented and analyzed. The effective mass is calculated from Eq. (2.2). The parameters required for this equation and the 2-DOF robot are defined as follows.

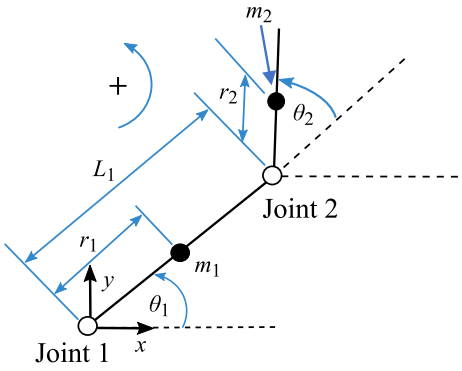

Fig. 2. The 2-DOF planar manipulator.

The inertia matrix for the 2-DOF manipulator is defined as follows [11, 12]:

$$\mathbf{M}(\theta) = \begin{bmatrix} \alpha + 2\beta c_2 & \delta + \beta c_2 \\ \delta + \beta c_2 & \delta \end{bmatrix}, \tag{4.1}$$

where $\alpha = I_{z1} + I_{z2} + m_1 r_1^2 + m_2 \left(L_1^2 + r_2^2\right)$, $\beta = m_2 L_1 r_2$, $\delta = I_{z2} + m_2 r_2^2$, and $c_2 = \cos(\theta_2)$.

The Jacobian matrix is defined as follows:

$$\mathbf{J} = \begin{bmatrix} -s_1 L_1 - L_2 s_{12} & -L_2 s_{12} \\ c_1 L_1 + L_2 c_{12} & L_2 c_{12} \end{bmatrix}, \tag{4.2}$$

where $c_1 = \cos(\theta_1)$, $s_1 = \sin(\theta_1)$, $s_{12} = \sin(\theta_1 + \theta_2)$, $c_{12} = \cos(\theta_1 + \theta_2)$.

The values of the parameters used to calculate the effective mass are taken from the datasheet of the KUKA LWR robot [13], as presented in Table 1.

Table 1. The values of the parameters of the 2-DOF manipulator used for calculating the effective mass [13].

Parameter	Value
L_1	0.39 m
r_1	0.195 m
L_2	0.156 m
r_2	0.078 m
m_1	3.3 kg
m_2	0.3 kg
I_{z1}	$0.1255\ \text{kg}\cdot\text{m}^2$
I_{z2}	$0.00183\ \text{kg}\cdot\text{m}^2$

To present the effective mass affected by the robot different configurations and end-effector position (d, h), the effective mass is calculated under different conditions; the first one by fixing d at a value and increasing h, whereas the second case by fixing h and increasing d. The direction vector u is selected to be $\mathbf{u} = [0 \quad -1]^{\mathrm{T}}$. The MATLAB code for calculating the effective mass for the 2-DOF robot is presented in Appendix 1.

4.1.1. First case: d is constant and h increases The results obtained from the first case where d is constant and h is increasing are presented in Figs 3 and 4. In the beginning, the inverse kinematics of the 2-DOF robot are calculated and

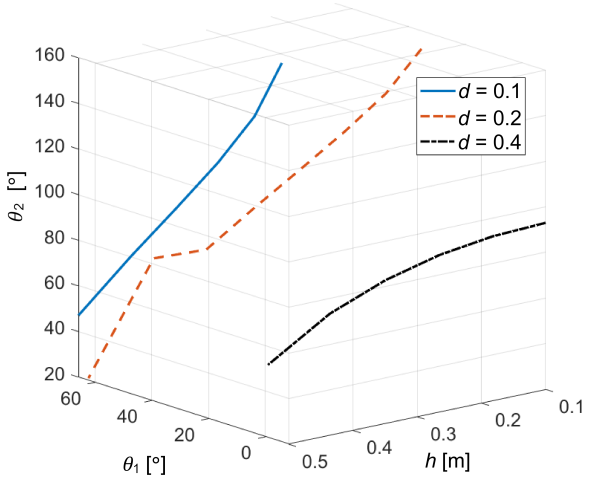

FIG. 3. The joints' positions of the 2-DOF robot (θ_1, θ_2) in the case of constant d and increasing h.

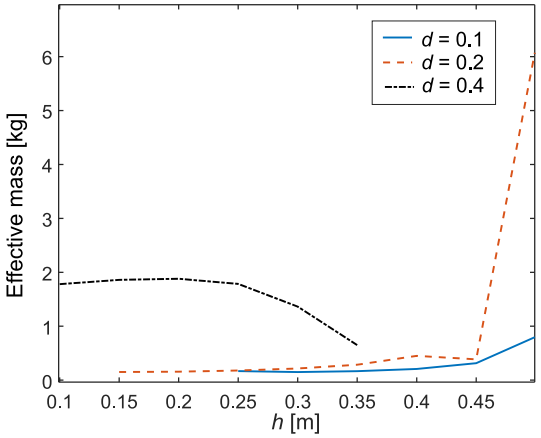

FIG. 4. The effective mass of the 2-DOF manipulator in the case of constant d and increasing h.

the robot joints' angles θ_1 and θ_2 are obtained (see Fig. 3) using the following three cases:

1) $d = 0.1$ m and $h = [0.1, 0.5]$ m.
2) $d = 0.2$ m and $h = [0.1, 0.5]$ m.
3) $d = 0.4$ m and $h = [0.1, 0.5]$ m.

After that, the robot effective mass is determined, as shown in Fig. 4.

From the results presented in Figs 3 and 4, the effective mass of the robot is changing with the change of the robot configurations and its end-effector position. With the increase of h, the effective mass of the robot is sometimes decreasing and sometimes increasing depending on the values and the directions of the robot joints' angles. In other words, we can say that the increase or the decrease in the robot effective mass depends on h and the directions and values of the robot joints' angles. One configuration of the 2-DOF robot from these results is presented in Fig. 5 with the direction vector $\mathbf{u}$.

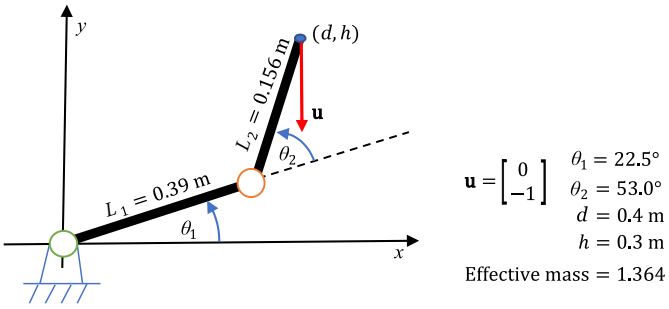

FIG. 5. The effective mass of the 2-DOF manipulator using one configuration from the many different robot configurations presented in Figs 3 and 4.

4.1.2. Second case: h is constant and d is increases The results obtained from the second case where h is constant and d increases are presented in Figs 6 and 7. In the beginning, the inverse kinematics of the 2-DOF robot are also calculated and the robot joints' angles θ_1 and θ_2 are obtained (see Fig. 6) using the following three cases:

1) $h = 0.1$ m and $d = [0.1, 0.5]$ m.
2) $h = 0.2$ m and $d = [0.1, 0.5]$ m.
3) $h = 0.4$ m and $d = [0.1, 0.5]$ m.

After that, the robot effective mass is determined, as shown in Fig. 7.

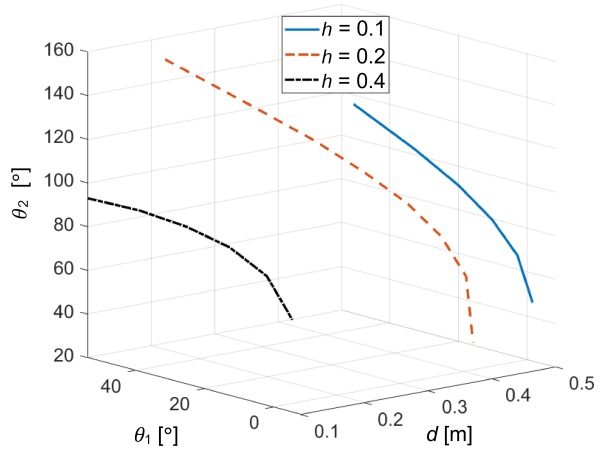

FIG. 6. The joints' positions of the 2-DOF robot (θ_1, θ_2) in the case of constant h and increasing d.

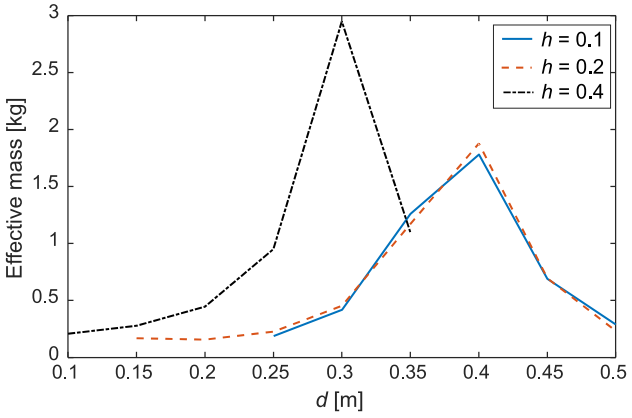

FIG. 7. The effective mass of the 2-DOF manipulator in the case of constant h and increasing d.

From the presented results, the effective mass of the robot is changing with the change of robot configurations and its end-effector position change. With the increase of d, the effective mass of the robot increases, then at a point it decreases depending on the values and the directions of the joints' angles of the robot. In other words, we can say that the increase or the decrease in the robot effective mass depends on h and the directions and the values of the joints' angles of the robot. One configuration of the 2-DOF robot from these results is presented in Fig. 8 with the direction vector $\mathbf{u}$.

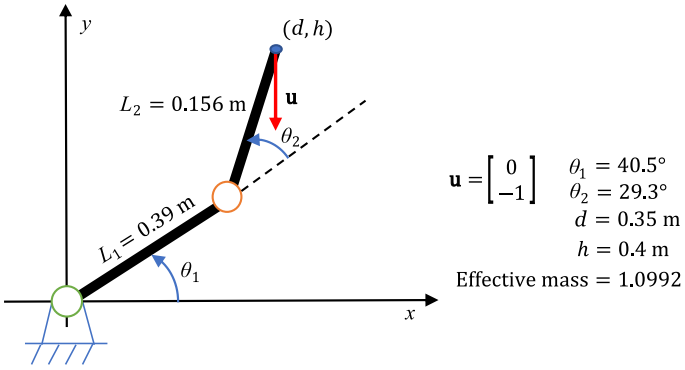

FIG. 8. The effective mass of the 2-DOF manipulator using one configuration from the many different robot configurations presented in Figs 6 and 7.

From the above results obtained from the analysis of the effective mass of the 2-DOF robot, we can conclude that the effective mass is associated with the robot configuration. Furthermore, it is related to the robot end-effector position.

In the next section, the analysis of the effective mass of the 3-DOF planar robot is presented.

4.2. The effective mass of the 3-DOF robot

In this subsection, the effective mass analysis of the 3-DOF planar manipulator (shown in Fig. 9) is presented and analyzed. The effective mass is calculated from Eq. (2.2). The parameters required for this equation and the 3-DOF robot are defined as follows.

The inertia matrix of the 3-DOF manipulator is defined as follows [14]:

$$\mathbf{M}(\theta) = \begin{bmatrix} M_{11} & M_{12} & M_{13} \\ M_{21} & M_{22} & M_{23} \\ M_{31} & M_{32} & M_{33} \end{bmatrix}, \tag{4.3}$$

where

$$M_{11} = \left(\frac{m_1}{3} + m_2 + m_3\right) L_1^2 + \left(\frac{m_2}{3} + m_3\right) L_2^2 + 2\left(\frac{m_2}{2} + m_3\right) L_1 L_2 \cos(\theta_2) + m_3 L_3 \left(L_1 \cos(\theta_2 + \theta_3) + L_2 \cos(\theta_3) + \frac{L_3}{3}\right),$$

$$M_{12} = M_{21} = \left(\frac{m_2}{3} + m_3\right) L_2^2 + \left(\frac{m_2}{2} + m_3\right) L_1 L_2 \cos(\theta_2) + m_3 L_3 \left(\frac{L_1}{2} \cos(\theta_2 + \theta_3) + L_2 \cos(\theta_3) + \frac{L_3}{3}\right),$$

$$M_{13} = M_{31} = m_3 L_3 \left(\frac{L_1}{2} \cos(\theta_2 + \theta_3) + \frac{L_2}{2} \cos(\theta_3) + \frac{L_3}{3}\right),$$

$$M_{22} = \left(\frac{m_2}{3} + m_3\right) L_2^2 + m_3 L_3 \left(L_2 \cos(\theta_3) + \frac{L_3}{3}\right),$$

$$M_{23} = M_{32} = m_3 L_3 \left(\frac{L_2}{2} \cos(\theta_3) + \frac{L_3}{3}\right),$$

$$M_{33} = \frac{m_3 L_3^2}{3}.$$

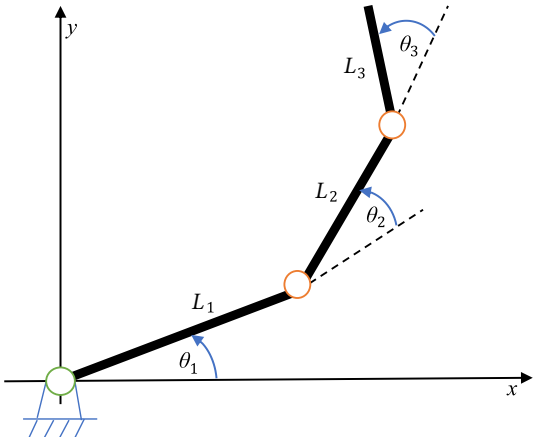

FIG. 9. The 3-DOF planar manipulator.

The Jacobian matrix is defined as follows:

$$\mathbf{J} = \begin{bmatrix} J_{11} & J_{12} & J_{13} \\ J_{21} & J_{22} & J_{23} \\ J_{31} & J_{32} & J_{33} \end{bmatrix}, \tag{4.4}$$

where

$$J_{11} = -L_2 \sin(\theta_1 + \theta_2) - L_1 \sin(\theta_1) - L_3 \sin(\theta_1 + \theta_2 + \theta_3),$$

$$J_{12} = -L_2 \sin(\theta_1 + \theta_2) - L_3 \sin(\theta_1 + \theta_2 + \theta_3),$$

$$J_{13} = -L_3 \sin(\theta_1 + \theta_2 + \theta_3),$$

$$J_{21} = L_2 \cos(\theta_1 + \theta_2) + L_1 \cos(\theta_1) + L_3 \cos(\theta_1 + \theta_2 + \theta_3),$$

$$J_{22} = L_2 \cos(\theta_1 + \theta_2) + L_3 \cos(\theta_1 + \theta_2 + \theta_3),$$

$$J_{23} = L_3 \cos(\theta_1 + \theta_2 + \theta_3),$$

$$J_{31} = J_{32} = J_{33} = 1.$$

The values of the parameters used to calculate the effective mass are taken from the datasheet of the KUKA LWR robot [13], as presented in Table 2. The same procedure followed with the 2-DOF manipulator is followed here with the 3-DOF. The effective mass is calculated using different robot configurations and end-effector position (d, h). The direction vector $\mathbf{u}$ is selected to be $\mathbf{u} = [0 \ -1 \ 0]^{\mathrm{T}}$. The MATLAB code for calculating the effective mass for the 3-DOF robot is presented in Appendix 2.

Table 2. The values of the parameters of the 3-DOF planar manipulator used for calculating the effective mass [13].

Parameter	Value
L_1	0.40 m
L_2	0.39 m
L_3	0.156 m
m_1	6.0 kg
m_2	5.0 kg
m_3	0.5 kg

4.2.1. First case: d is constant and h increases The results from the case where d is constant and h increases are presented in Figs 10 and 11. As discussed before, the inverse kinematics of the 3-DOF robot are calculated and the robot joints' angles θ_1, θ_2, and θ_3 are obtained[1)] (see Fig. 10) using the following three cases:

1) $d = 0.2$ m and $h = [0.05, 0.5]$ m,
2) $d = 0.4$ m and $h = [0.05, 0.5]$ m,
3) $d = 0.6$ m and $h = [0.05, 0.5]$ m.

After that, the effective mass of the robot is determined, as shown in Fig. 11.

[1)] Note: Many possible values of the three angles result in the same effector position (d, h) but different geometric configurations. Any set of angles can be used in the analysis to illustrate the concept that the effective mass changes with the change of the joints' angles.

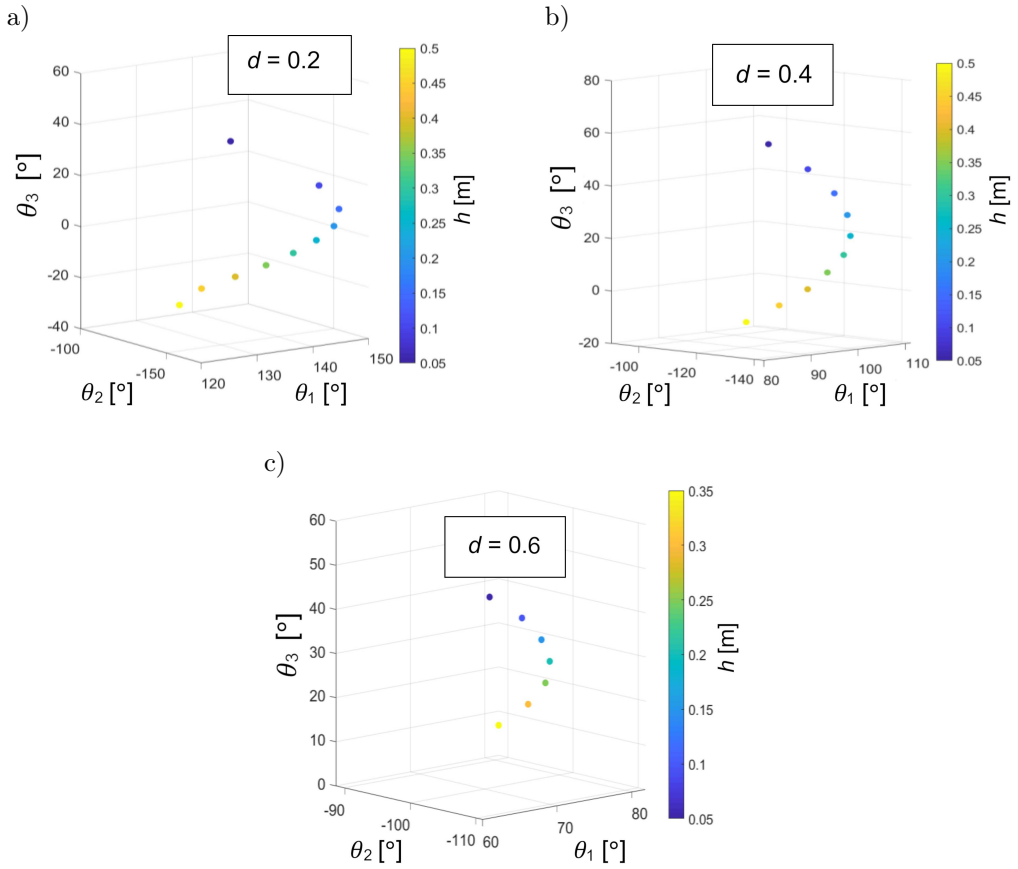

FIG. 10. The joints' positions of the 3-DOF robot ($(\theta_1, \theta_2, \theta_3)$ in the case of constant d and increasing h: a) $d = 0.2$ m, b) $d = 0.4$ m, and c) $d = 0.6$ m.

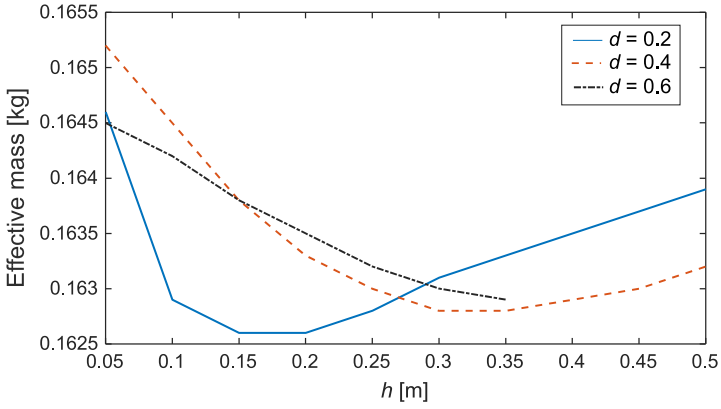

FIG. 11. The effective mass of the 3-DOF planar manipulator in the case of constant d and increasing h.

From the results presented in Figs 10 and 11, the effective mass of the robot changes with the change of the robot configurations and end-effector position. With the increase of h, the effective mass of the robot decreases, and then at a point it increases depending on the values and directions of the robot joints' angles (θ_1, θ_2, θ_3). In other words, we can say that the decrease or the increase in the effective mass of the 3-DOF robot depends on h and the directions and values of the joints' angles of the robot. One configuration of the 3-DOF planar robot from these results is presented in Fig. 12 with the direction vector $\mathbf{u}$.

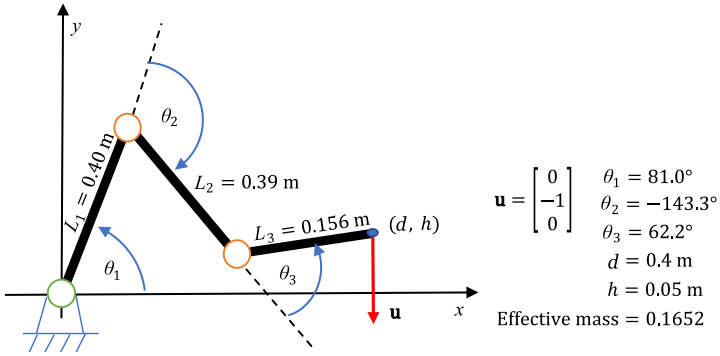

FIG. 12. The effective mass of the 3-DOF planar manipulator using one configuration from the many different robot configurations presented in Figs 10 and 11.

4.2.2. Second case: h is constant and d increases The obtained results from the case where h is constant and d increases are presented in Figs 13 and 14. The inverse kinematics of the 3-DOF robot are calculated and the robot joints' angles θ_1, θ_2, and θ_3 are obtained (see Fig. 13) using the following three cases:

1) $h = 0.2$ m and $d = [0.05, 0.5]$ m,
2) $h = 0.4$ m and $d = [0.05, 0.5]$ m,
3) $h = 0.6$ m and $d = [0.05, 0.5]$ m.

After that, the effective mass of the robot is determined, as shown in Fig. 14.

From the presented results, the effective mass of the robot changes with the change of the robot configurations and end-effector position. With the increase of d, the effective mass of the robot decreases, and then at the end, it slightly increases depending on the values and directions of the robot joints' angles (θ_1, θ_2, θ_3). We can say that the decrease or increase in the effective mass of the 3-DOF robot depends on d and the directions and the values of the robot joints' angles. One configuration of the 3-DOF planar robot from these results is presented in Fig. 15 with the direction vector $\mathbf{u}$.

It should be stated that the effective mass of the 2-DOF and 3-DOF robot is investigated by increasing both d and h simultaneously of the robot end-effector. The results are in the same prediction as the results presented in this

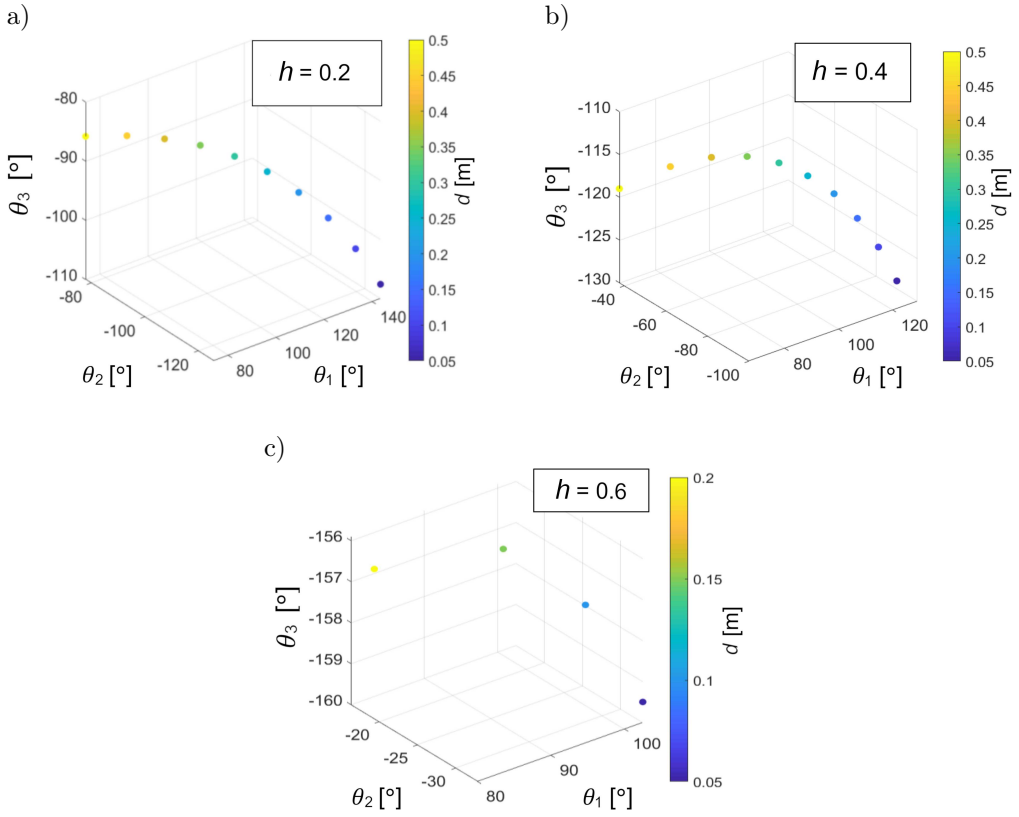

FIG. 13. The joints' positions of the 3-DOF robot (θ_1, θ_2, θ_3) in the case of constant h and increasing d: a) $h = 0.2$ m, b) $h = 0.4$ m, c) $h = 0.6$ m.

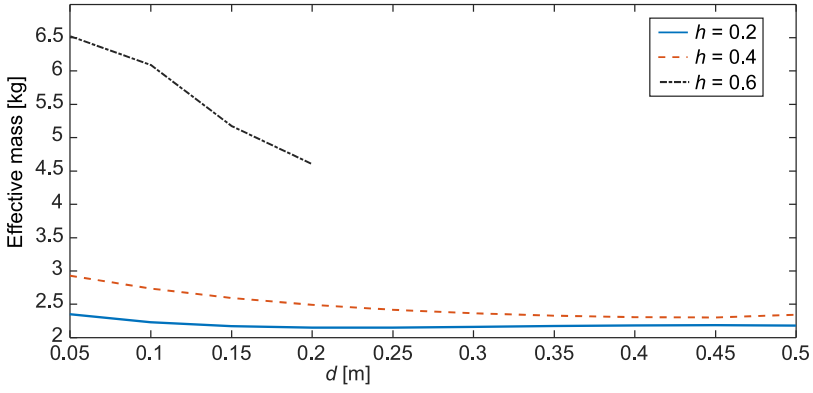

FIG. 14. The effective mass of the 3-DOF planar manipulator in the case of constant h and increasing d.

section. The results illustrate that the effective mass sometimes decreases and sometimes increases depending on the values and directions of the robot joints' angles.

We conclude from the obtained results that the effective mass of the robot depends on the robot configurations and the t end-effector position.

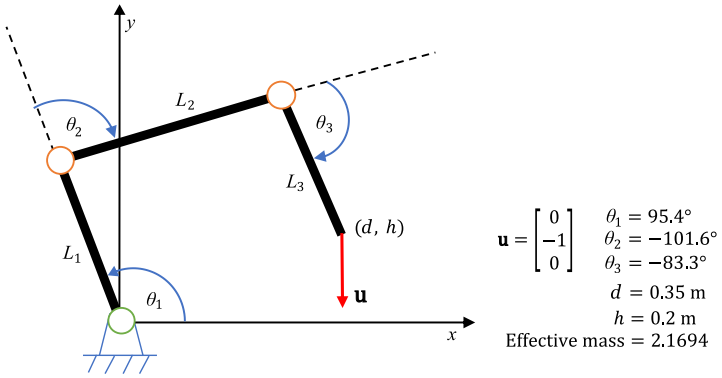

Fig. 15. The effective mass of the 3-DOF planar manipulator using one configuration from the many different robot configurations presented in Figs 13 and 14.

5. Conclusions and future work

This study presented the mathematical analysis of the effective mass of the robot and its ellipsoid. The effective mass of the robot was investigated with the external force (collision) affecting the robot end-effector. The results of this investigation prove that the collision force depends on the robot effective mass. The effective mass was analyzed using different robot configurations and different positions from the robot end-effector. The 2-DOF and 3-DOF planar robots were used for this analysis. The results from this analysis prove that the robot effective mass is related to the robot configurations and end-effector position. By increasing the position of the robot end-effector in the x-axis only, y-axis only, or both x-axis and y-axis, the effective mass of the robot sometimes decreases and sometimes increases depending on the values and the directions of the joints' angles of the robot.

The promising results need further investigations for the robot effective mass examined in a more dense workspace. The experimental work can be achieved by moving the robot in different configurations and then the effective mass can be calculated and checked. The effective mass of the robot during its joint space motion can also be analyzed. In addition, the analysis using 6-DOF and 7-DOF manipulator can be applied. Effective mass can therefore be considered one of the criteria in optimizing robot kinematics and configuration.

Appendix 1. The MATLAB code for calculating the effective mass of the 2-DOF robot

The implemented MATLAB code to calculate the effective mass of the 2-DOF robot is presented as follows:

```
% Effective mass of the 2-DOF robot
% Author: Abdel-Nasser Sharkawy
%%
clc
clear all;

% Define the parameters
L1 = sym('L1', 'real');
L2 = sym('L2', 'real');
r1 = sym('r1', 'real');
r2 = sym('r2', 'real');

m1 = sym('m1', 'real');
m2 = sym('m2', 'real');

Iz1 = sym('Iz1', 'real');
Iz2 = sym('Iz2', 'real'|);

theta1 = sym('theta1', 'real');
theta2 = sym('theta1', 'real');

%dimensions from Kuka robot
L1 = 0.39; %m
L2 = 0.156; %m
r1 = 0.5 * L1; %m
r2 = 0.5 * L2; %m
m1 = 3.3; %kg
m2 = 0.3; %kg
Iz1 = m1 * r1^2; %kg.m^2
Iz2 = m2 * r2^2; %kg.m^2
theta1 = 40.5*pi/180 %Angle is converted from deg to rad
theta2 = 29.3*pi/180

%%
%The main program
alpha = Iz1 + Iz2 + m1 * r1^2 + m2 *(L1 ^2 + r2^2);
beta = m2 * L1 * r2;
Zelta = Iz2 + m2 * r2^2;

inertia = [(alpha + 2 * beta * cos(theta2)) (Zelta + beta * cos(theta2));
  (Zelta + beta * cos(theta2)) Zelta];

Jacobian = [(-sin(theta1) * L1 - L2 * sin(theta1 + theta2))
  (-L2 * sin(theta1 + theta2));
(cos(theta1) * L1 + L2 * cos(theta1 + theta2)) (L2 * cos(theta1 + theta2))];
u = [0 -1]';

Effective_mass = 1/(transpose(u)*Jacobian*inv(inertia)*transpose(Jacobian)* u)
```

Appendix 2. The MATLAB code for calculating the effective mass of the 3-DOF planar robot

The implemented MATLAB code to calculate the effective mass of the 3-DOF planar robot is presented as follows:

```
% Effective mass of the 3-DOF planar robot
% Author: Abdel-Nasser Sharkawy
%%
clc
clear all;

% Define the parameters
L1 = sym('L1', 'real');
L2 = sym('L2', 'real');
L3 = sym('L3', 'real');

r1 = sym('r1', 'real');
r2 = sym('r2', 'real');
r3 = sym('r3', 'real');

m1 = sym('m1', 'real');
m2 = sym('m2', 'real');
m3 = sym('m2', 'real');

I1 = sym('I1', 'real');
I2 = sym('I2', 'real');
I3 = sym('I3', 'real');

theta1 = sym('theta1', 'real');
theta2 = sym('theta2', 'real');
theta2 = sym('theta3', 'real');

%dimensions from Kuka robot
L1 = 0.40;
L2 = 0.39;
L3 = 0.156;
r1 = 0.5 * L1;
r2 = 0.5 * L2;
r3 = 0.5 * L3;
m1 = 6;
m2 = 5;
m3 = 0.5;
I1 = m1 * r1^2;
I2 = m2 * r2^2;
I3 = m3 * r2^2;

% theta1 = 70*pi/180;
% theta2 = 170*pi/180;
% theta3 = 145*pi/180;

theta1 = 2.35689009782608 %rad
theta2 = -2.16767562594963 %rad
theta3 = -1.76001079867135 %rad
```

```
%%
%The main program
M11 = ((m1/3) + m2 + m3) * L1^2 + (m2/3 + m3) * L2^2 + 2 * (m2/2 + m3) * L1 * L2 *
cos (theta2) + m3 * L3 * (L1 * cos (theta2 + theta3) + L2 * cos(theta3) + L3/3);
M12 = ((m2/3) + m3) * L2^2 + (m2/2 + m3) * L1 * L2 * cos(theta2) + m3 * L3 *
((L1/2) * cos(theta2 + theta3) + L2 * cos(theta3) + L3/3);
M21 = ((m2/3) + m3) * L2^2 + (m2/2 + m3) * L1 * L2 * cos(theta2) + m3 * L3 *
((L1/2) * cos(theta2 + theta3) + L2 * cos(theta3) + L3/3);
M13 = m3 * L3 * ((L1/2) * cos(theta2 + theta3) + (L2/2) * cos(theta3) + (L3/3));
M31 = m3 * L3 * ((L1/2) * cos(theta2 + theta3) + (L2/2) * cos(theta3) + (L3/3));
M22 = ((m2/3) + m3) * L2^2 + m3 * L3 * (L2 * cos(theta3) + (L3/3));
M23 = m3 * L3 * ((L2/2) * cos(theta3) + L3/3);
M32 = m3 * L3 * ((L2/2) * cos(theta3) + L3/3);
M33 = (m3 * L3^2)/3;

inertia = [M11 M12 M13;
  M21 M22 M23;
  M31 M32 M33];

J11 = -L2 * sin(theta1 + theta2) - L1 * sin(theta1) - L3 *
sin(theta1 + theta2 + theta3);
J12 = -L2 * sin(theta1 + theta2) - L3 * sin(theta1 + theta2 + theta3);
J13 = - L3 * sin(theta1 + theta2 + theta3);
J21 = L2 * cos(theta1 + theta2) + L1 * cos(theta1) + L3 *
cos(theta1 + theta2 + theta3);
J22 = L2 * cos(theta1 + theta2) + L3 * cos(theta1 + theta2 + theta3);
J23 = L3 * cos(theta1 + theta2 + theta3);
J31 = 1;
J32 = 1;
J33 = 1;

Jacobian = [J11 J12 J13;
J21 J22 J23;
J31 J32 J33];
u = [0 -1 0]';

Effective_mass = 1/(transpose(u)*Jacobian*inv(inertia)*transpose(Jacobian)* u)
```

Acknowledgments

The author would like to thank Assistant Professor Matej Hoffmann and his group in the Department of Cybernetics, Faculty of Electrical Engineering, Czech Technical University in Prague, for their help and support in preparing this paper. This group greatly helped the author to obtain the inverse kinematics of the 3-DOF planar manipulator.

Conflict of interest

The author states that there is no conflict of interest.

References

1. Khatib O., Inertial properties in robotic manipulation: an object-level framework, *The International Journal of Robotics Research*, **14**(1): 19–36, 1995, doi: 10.1177/027836499501400103.

2. Lee S.-D., Kim B.-S., Song J.-B., Human-robot collision model with effective mass and manipulability for design of a spatial manipulator, *Advanced Robotics*, **27**(3): 189–198, 2013, doi: 10.1080/01691864.2012.754076.

3. Chen G., Liu D., Wang Y., Jia Q., Liu X., Contact force minimization for space flexible manipulators based on effective mass, *Journal of Guidance, Control, and Dynamics*, **42**(8): 1870–1877, 2019, doi: 10.2514/1.G003987.

4. Mavrakis N., Ghalamzan E.A.M., Stolkin R., Safe robotic grasping: Minimum impact-force grasp selection, [in:] *IEEE/RSJ International Conference on Intelligent Robots and Systems (IROS)*, pp. 4034–4041, 2017, doi: 10.1109/IROS.2017.8206258.

5. Lämmle A., Development of a new mechanic safety coupling for human robot collaboration using magnetorheological fluids, *Procedia CIRP*, **81**: 908–913, 2019, doi: 10.1016/j.procir.2019.03.226.

6. Shin H., Kim S., Seo K., Rhim S., A virtual pressure and force sensor for safety evaluation in collaboration robot application, *Sensors* (Basel), **19**(19): 1–11, 2019, doi: 10.3390/s19194328.

7. Vemula B., Matthias B., Ahmad A., A design metric for safety assessment of industrial robot design suitable for power- and force-limited collaborative operation, *International Journal of Intelligent Robotics and Applications*, **2**(2): 226–234, 2018, doi: 10.1007/s41315-018-0055-9.

8. Hunt K.H., Crossley F.R.E., Coefficient of restitution interpreted as damping in vibroimpact, *Journal of Applied Mechanics*, **42**(2): 440–445, 1975, doi: 10.1115/1.3423596.

9. Povse B., Koritnik D., Bajd T., Munih M., Correlation between impact-energy density and pain intensity during robot-man collision, [in:] *2010 3rd IEEE RAS & EMBS International Conference on Biomedical Robotics and Biomechatronics*, pp. 179–183, 2010, doi: 10.1109/BIOROB.2010.5626073.

10. Lee S.-D., Song J.-B., Guideline for determination of link mass of a robot arm for collision safety, [in:] *8th International Conference on Ubiquitous Robots and Ambient Intelligence (URAI)*, pp. 383–385, 2011, doi: 10.1109/URAI.2011.6145847.

11. Murray R.M., Li Z., Sastry S.S., *A Mathematical Introduction to Robotic Manipulation*, CRC Press, 1994.

12. Sharkawy A.-N., Koustoumpardis P.N., Dynamics and computed-torque control of a 2-DOF manipulator: Mathematical analysis, *International Journal of Advanced Science and Technology*, **28**(12): 201–212, 2019.

13. KUKA Roboter GmbH, *Lightweight Robot 4+, Specification*, D-86165 Augsburg, Germany, 2010.

14. Van Nguyen T., Dumitriu D.N., Stroe I., Controlling the motion of a planar 3-DOF manipulator using PID controllers, *INCAS Bulletin*, **9**(4): 91–99, 2017, doi: 10.13111/2066-8201.2017.9.4.8.

Received March 6, 2021; accepted version July 11, 2021.
